Hybrid simulations in application to NSTX, FRCs, and basic plasma physics

Elena Belova

PPPL

April 7 , 2017

HYM – HYbrid and MHD code

Applications

- NSTX
  - Sub-cyclotron frequency Alfven eigenmodes (GAE and CAE)
- ICC Theory and Modeling
  - Hybrid simulations of spheromak merging
  - Effects of beam ions on stability
  - FRC – Tri-Alpha collaboration
  - Rotation control
  - n=2 rotational and n=1 wobble modes

Code description

- 3-D nonlinear.
- Physical models:
  - Resistive MHD & Hall-MHD
  - Hybrid (fluid electrons, particle ions)
  - MHD/particle (one-fluid thermal plasma, + energetic particle ions)
  - Drift-kinetic particle electrons
- Full-orbit kinetic ions.
- For particles: delta-f / full-f numerical scheme.
- Parallel (3D domain decomposition, MPI)

Fast ions – delta-f scheme: $F_0=F_0(\varepsilon,\mu,p_\varphi)$

Equilibrium distribution function $F_0 = F_1(v)\, F_2(\lambda)\, F_3(p_\varphi, v)$

$$F_1(v) = \frac{1}{v^3 + v_*^3}, \quad \text{for} \quad v < v_0$$

$$F_2(\lambda) = \exp\left(-(\lambda - \lambda_0)^2 / \Delta\lambda^2\right)$$

$$F_3(p_\phi, v) = \frac{(p_\phi - p_0)^\beta}{(R_0 v - \psi_0 - p_0)^\beta}, \quad \text{for} \quad p_\phi > p_0$$

where $v_0 = 2\text{-}5 v_A$, $v_* = v_0/2$, $\lambda = \mu B_0/\varepsilon$ – pitch angle parameter, $\lambda_0 = 0.5\text{-}0.7$, and $\mu = \mu_0 + \mu_1$ includes first-order corrections [Littlejohn'81]:

$$\mu = \frac{(\mathbf{v}_\perp - \mathbf{v}_\mathbf{d})^2}{2B} - \frac{\mu_0 v_\parallel}{2\mathrm{B}}[\hat{b}\cdot\nabla\times\hat{b} - 2(\hat{a}\cdot\nabla\hat{b})\cdot\hat{c}]$$

$\mathbf{v}_d$ is magnetic gradient and curvature drift velocity, $\hat{c} = \mathbf{v}_\perp/v_\perp$, $\hat{a} = \hat{b}\times\hat{c}$.

Parameters are chosen to match TRANSP beam profiles.

HYM simulations reproduce frequency range of unstable GAE and CAE modes observed in NSTX

Experimental analysis:

Detailed measurements of GAE and CAE amplitudes and mode structure for H-mode plasma in NSTX shot 141398 [N. Crocker, NF 2013].

- **CAEs**: f>600 kHz, and |n|≤5.
- **GAEs**: f<600 kHz, and |n|~6-8.
- Co- and counter-rotating CAEs with f~1.2-1.8 MHz, and n=6-14 also observed in the same shot [E. Fredrickson, PoP 2013].

HYM simulations:

- For n=5-7 most unstable are counter-rotating GAEs, with f= 380-550 kHz.
- For n=4 and n=8, 9 most unstable are co-rotating CAEs with f= 870-1200 kHz.

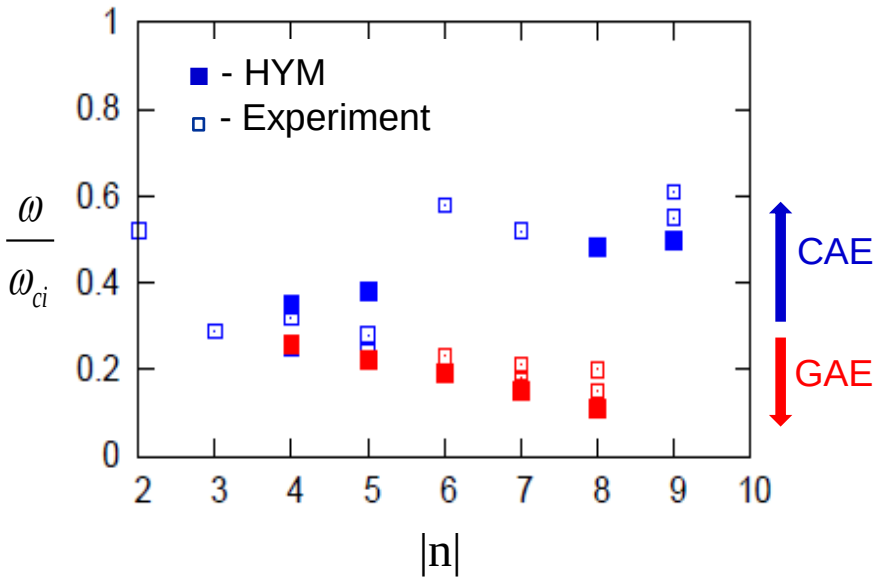

Frequency versus toroidal mode number for unstable GAEs (red) and CAEs (blue), from HYM simulations and experiment, f_{ci}=2.5MHz.

CAE has large compressional component in the core and couples to KAW

n=4, CAE

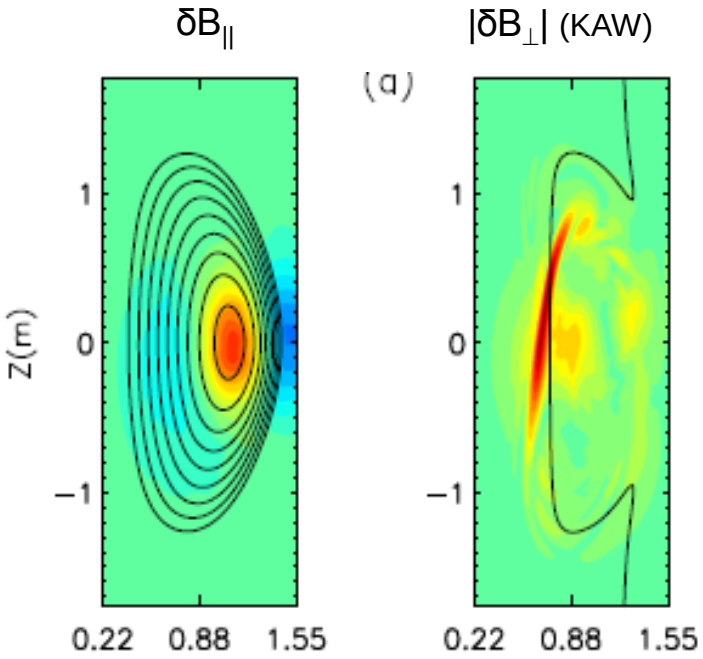

$\delta B_{||}$ is significantly larger than $\delta B_{\perp}$ at the axis.

n=6, GAE

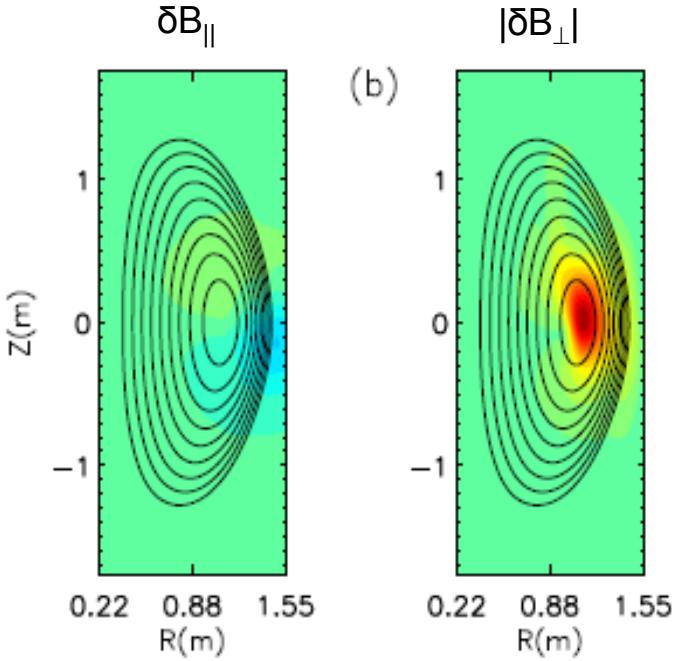

$\delta B_{||}$ is comparable to $\delta B_{\perp}$ only at the edge.

- CAE/KAW coupling seen for all unstable CAEs.
- KAW has large amplitude on HFS.

On-axis CAE couples to off-axis KAW

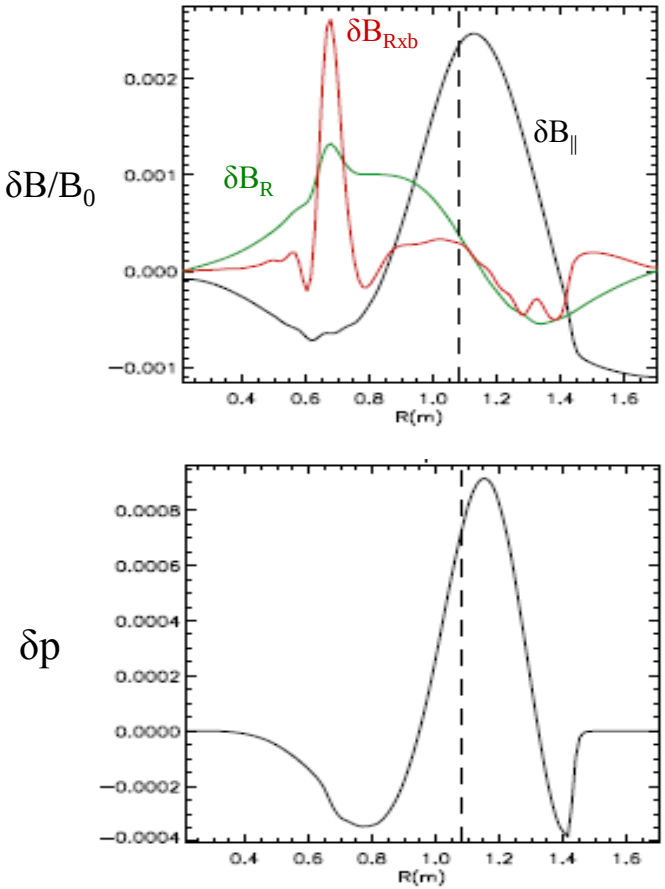

Profiles of (a) magnetic field perturbation; and (b) normalized thermal δp for the n=4 CAE versus major radius. The CAE peaks near the magnetic axis R=1.07m.

- Radial width of KAW is determined by beam ions Larmor radius, $k_{\perp} \sim 1/\Delta = (L\rho^2)^{-1/3}$, where $\rho^2 = \left(\frac{3}{4}\left[1+\frac{\beta_b}{\beta_i}\right]+\frac{T_e}{T_i}\right)\rho_i^2$ (full kinetic model), and
  $\rho = \sqrt{3/4\, n_b/n_e}\;\rho_b$ (HYM model).
- Resonant mode polarization is consistent with KAW mode, ie
  $\delta B_Z >> \delta B_R, \delta B_{||}$ and $\delta V_Z >> \delta V_R, \delta V_{||}$ with $\delta V_Z \sim -\delta B_Z$.
- $\delta B_{||}$, δp and δn show a smooth behavior across the resonance, consistent with incompressible nature of KAW.
- Resonance with KAW is located at the edge of CAE well, near the edge beam ion density profile at r/a~0.6.

NSTX-U

PPPL PRINCETON PLASMA PHYSICS LABORATORY

Simulations: main drive for CAE comes from resonant particles with $v_{||} \sim \omega/k_{||}$

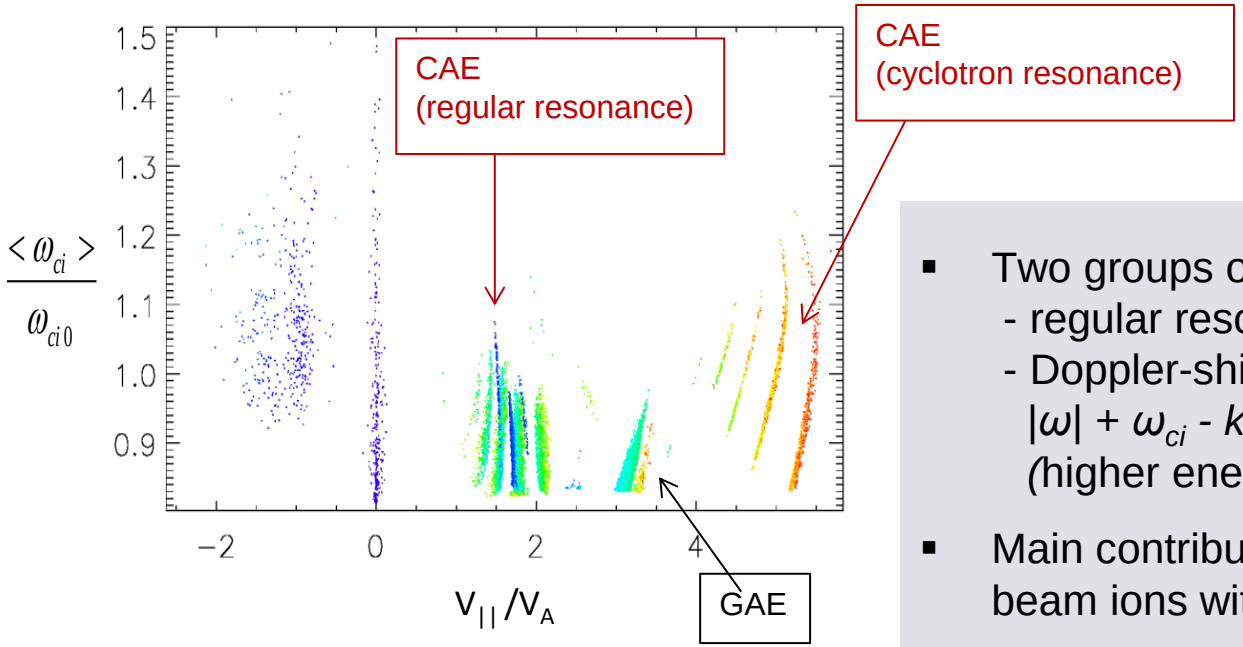

Orbit-averaged cyclotron frequency vs orbit-averaged parallel velocity for resonant particles. From simulations for n=8 CAE (ω=0.48ω_{ci0}, γ=0.004ω_{ci0}).
Particle color corresponds to different energies: from E=0 (purple) to E= 90keV (red).

- Two groups of resonant particles:
  - regular resonance: $\omega - k_{||}v_{||} = 0$,
  - Doppler-shifted cyclotron resonance: $|\omega| + \omega_{ci} - k_{||}v_{||} = 0$ (higher energy particles).
- Main contribution comes from the beam ions with $v_{||} \sim \omega/k_{||}$.
- "Turning off" high-energy resonant particles does not change the growth rate → contribution from the cyclotron resonances is negligible.

Location of resonant particles in phase-space

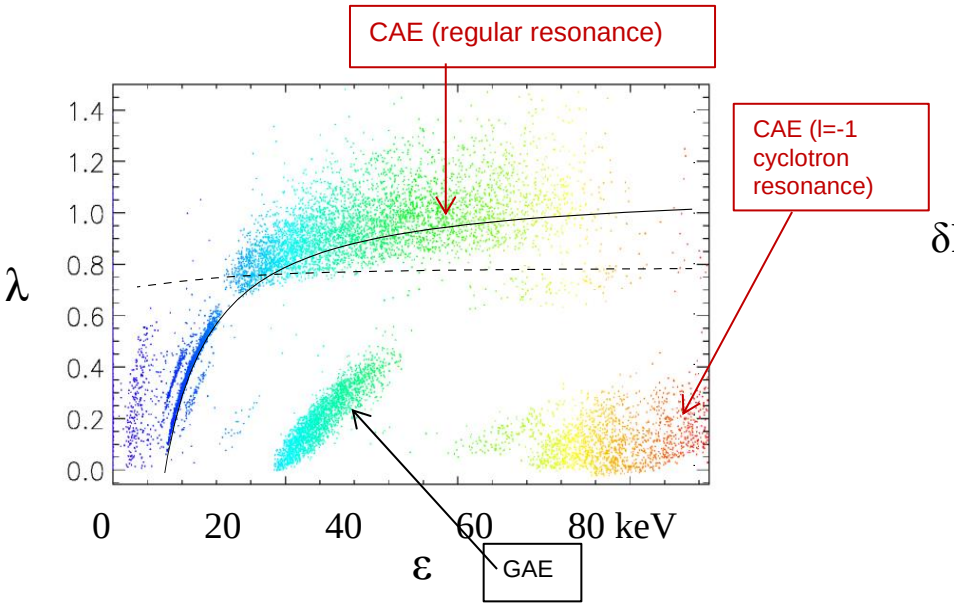

Location of resonant particles in phase space: $\lambda=\mu B_0/\varepsilon$ vs energy. From HYM simulations for n=8 CAE. Particle color corresponds to different energies: from E=0 (purple) to E=90keV (red).

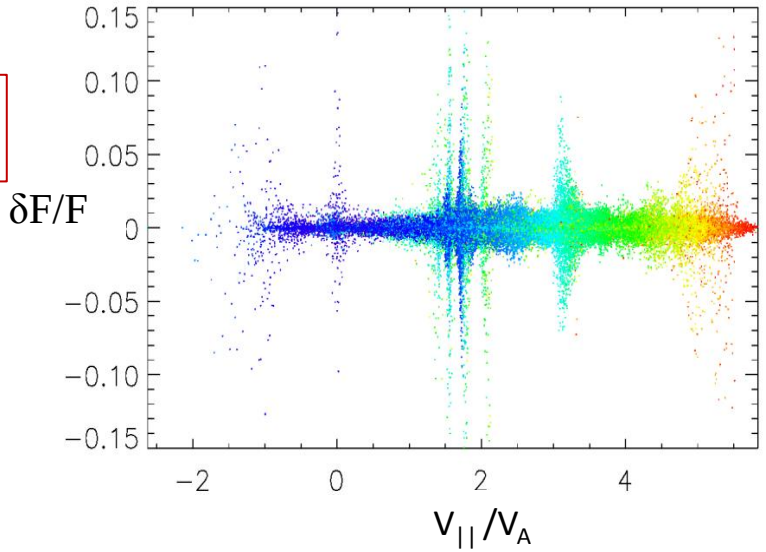

Particle weight $w \sim \delta F/F$ vs orbit-averaged parallel velocity for all simulations particles.

- Resonant velocity $v_{||} \approx \omega R_0/n = 1.7 V_A$, in good agreement with simulations.
- Distribution in (λ, ε) space can be described approximately by a relation $\lambda = 1 - v_{||}^2/2\varepsilon$ for a fixed $v_{||}$ (solid line plotted for $v_{||} = 1.7V_A$).
- Instability is driven mostly by large-λ beam ions with $D = \frac{\partial F_0}{\partial \varepsilon} - \frac{\lambda}{\varepsilon}\frac{\partial F_0}{\partial \lambda} > 0$, whereas lower-energy passing ions are stabilizing (dashed line corresponds to condition D=0).

Nonlinear simulations show CAE saturation amplitudes higher than experimentally observed

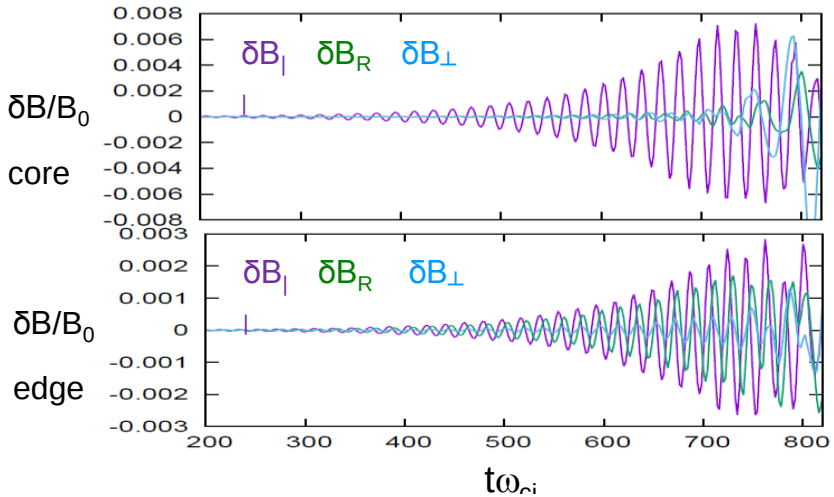

Time evolution of $dB_{||}$ and two components of $\delta\mathbf{B}_{\perp}$ in the core, and close to the plasma edge on LFS.

- In the core, the compressional perturbation is 3-4 times larger than the shear perturbation.
- Mixed compressional/shear polarization near the plasma edge on LFS .

- Saturation amplitude of the n=4 CAE: $\delta B_{||}/B_0 = 6.6\times10^{-3}$.
- Measured displacement $|\xi| = 0.1$-0.4 mm corresponds to $\delta n/n_0 <\sim 10^{-3}$ [Crocker,17].

Significant fraction of the total beam power can transferred to a single CAE of relatively large amplitude

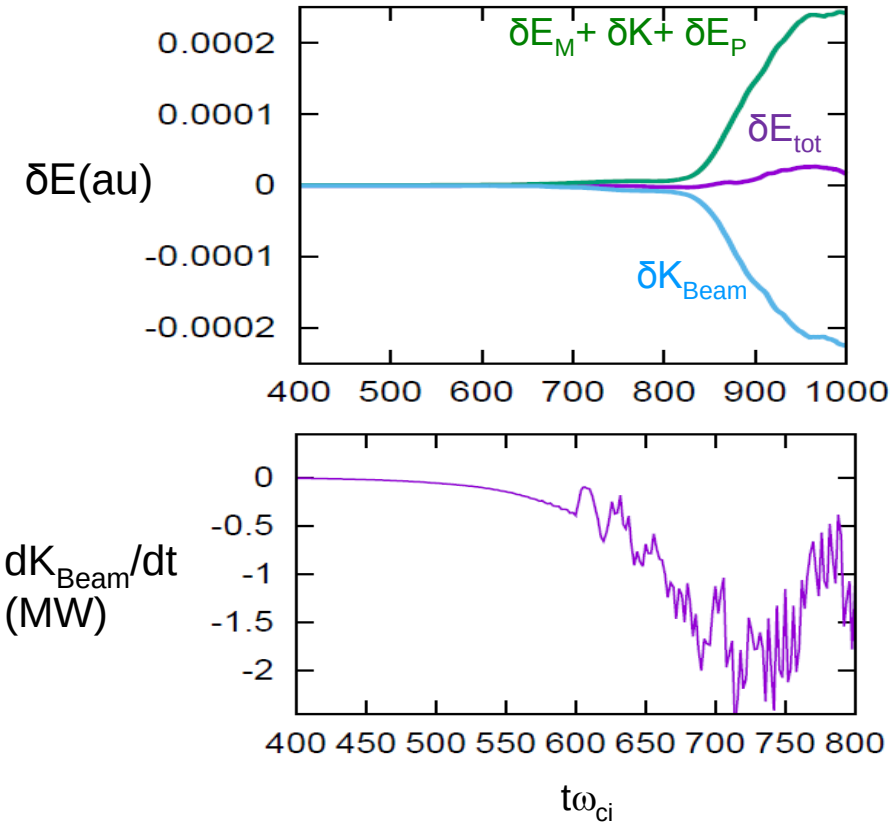

(a) Time evolution of the fluid energy (green), the beam ion energy (light blue), and the total energy of the system (purple);

(b) Time evolution of rate of change of beam ion energy, calculated as $\int (\mathbf{J}_{beam}\mathbf{E})\, d^3x$.

Rate of change of the beam ion energy is ~1.5MW for calculated the n=4 CAE saturation amplitude $\delta B_{||}/B_0 = 6.6\times10^{-3}$.

Energy flux is directed away from magnetic axis

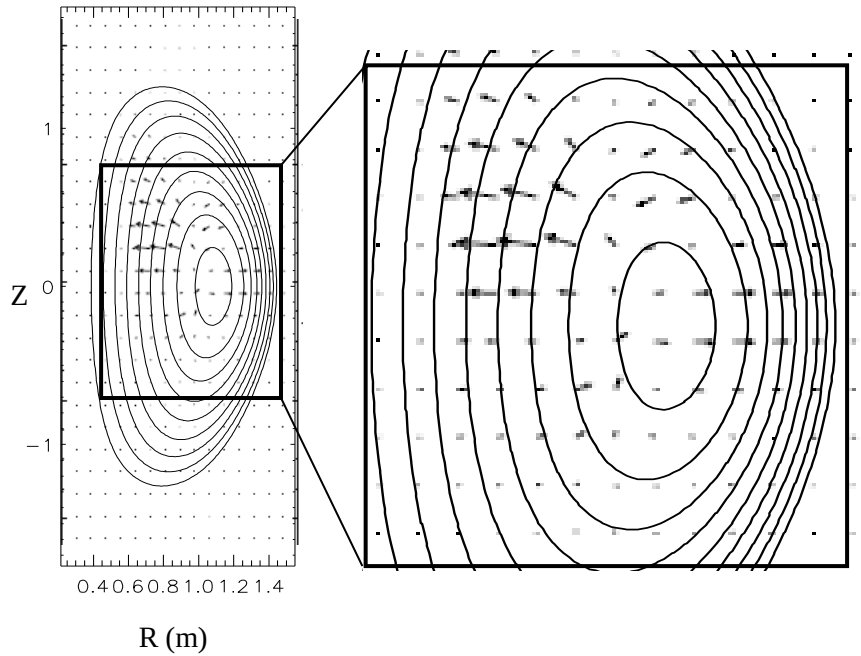

Change of energy flux across resonant layer at R~0.7m is $S_R \sim 0.8\times10^5$ W/m^2,which corresponds to power absorption at the high-field-side resonance of P~ 0.2 MW for $\delta B_{||}/B_0 \sim 3\times10^{-3}$.

Vector plot of energy flux $\mathbf{S} = \mathbf{E}\times\mathbf{B}/4\pi + p\mathbf{V}\gamma/(\gamma-1)$.

Energy flux is directed away from magnetic axis, towards both high- and low-field side. LFS resonance is more diffuse compared to HFS.

From the self-consistent nonlinear simulations of the n=4 CAE mode near saturation.

CAE-to-KAW energy channeling shows strong scaling with the beam power

- From density threshold – damping rate due to CAE/KAW coupling is large γ_{damp}= 0.66 $\gamma_{dr.}$
- Threshold value of the beam power needed for the excitation of the n=4 CAE can be estimated as P~4MW.
- Instability saturates nonlinearly due to particle trapping, and $\delta B_{||}/B_0 \sim (\gamma/\omega_{ci})^2$.
- Absorption rate shows a very strong scaling with growth rate: $\Delta S \sim (\gamma/\omega_{ci})^5$, implying that the energy loss at the resonance scales as a fifth power of the beam ion density (beam power).

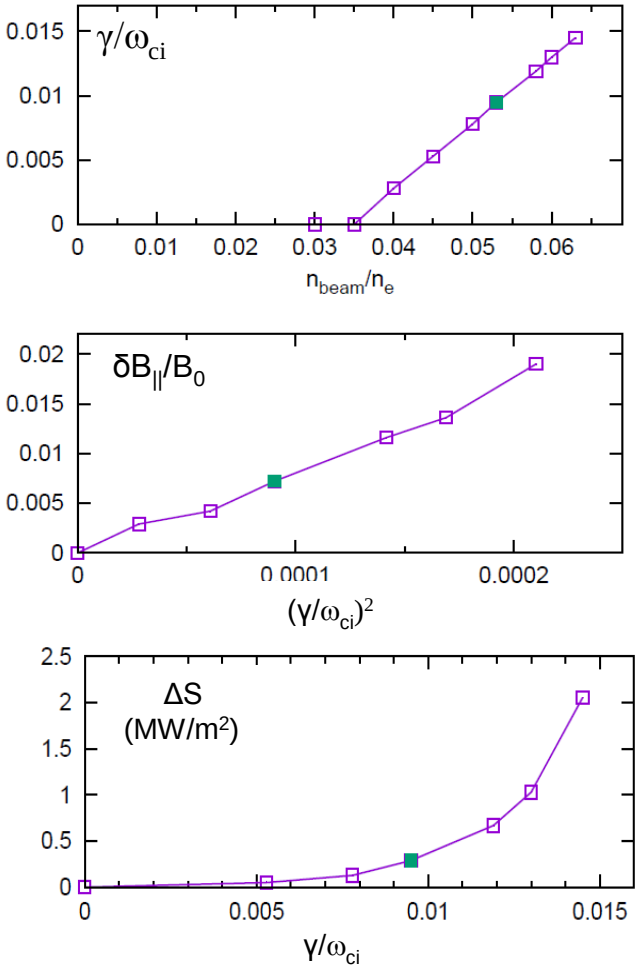

(a) Growth rate of the n=4 CAE vs beam ion density
(b) Saturation amplitude vs γ^2
(c) Calculated change of the energy flux at the resonance location vs γ

NSTX-U simulations: GAE stabilization

HYM simulations reproduce experimental finding: off-axis neutral beam injection reliably and strongly suppresses unstable GAEs

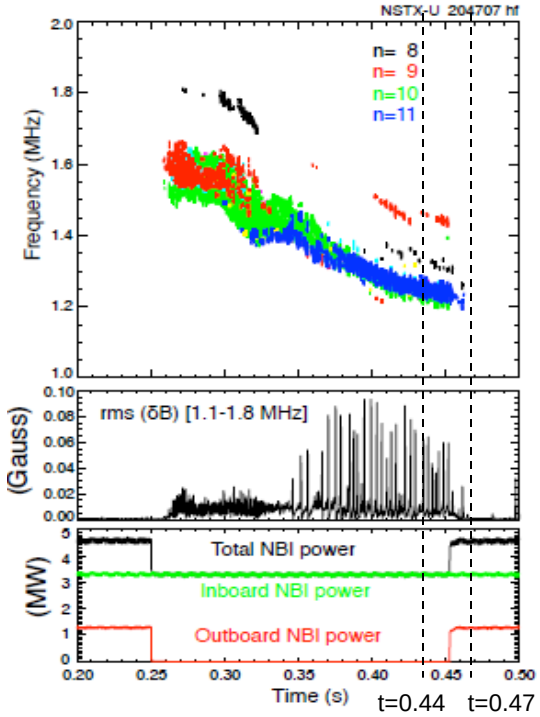

(a) Spectrogram on magnetic fluctuations (n=8-11 counter-GAEs).
(b) Rms magnetic fluctuations;
(c) Injected beam power.

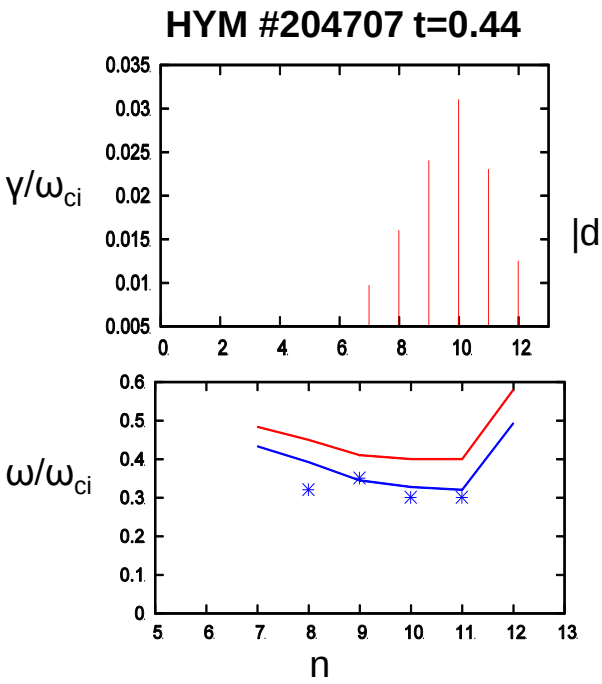

(a) Growth rates and (b) frequencies of unstable counter-GAEs from HYM simulations for t=0.44s. Blue line is Doppler-shift corrected frequencies, points – experimental values.

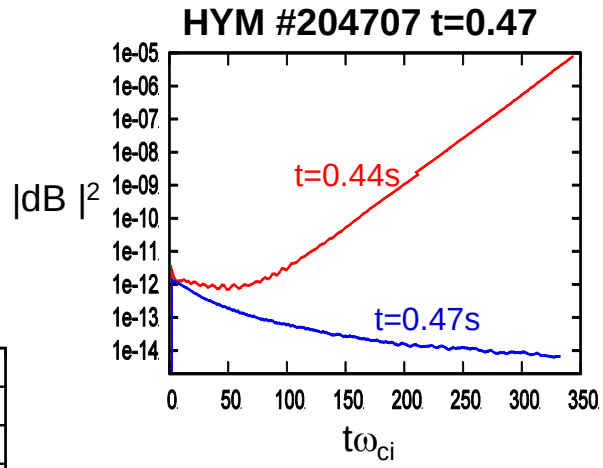

Time evolution of magnetic energy of n=10 GAE from HYM simulations for t=0.44s (red), and t=0.47s (blue).

HYM shows complete stabilization of n= 7-12 counter-GAEs by additional off-axis beam injection.

NSTX-U

PPPL PRINCETON PLASMA PHYSICS LABORATORY

NSTX-U simulations: profile and F_b fits

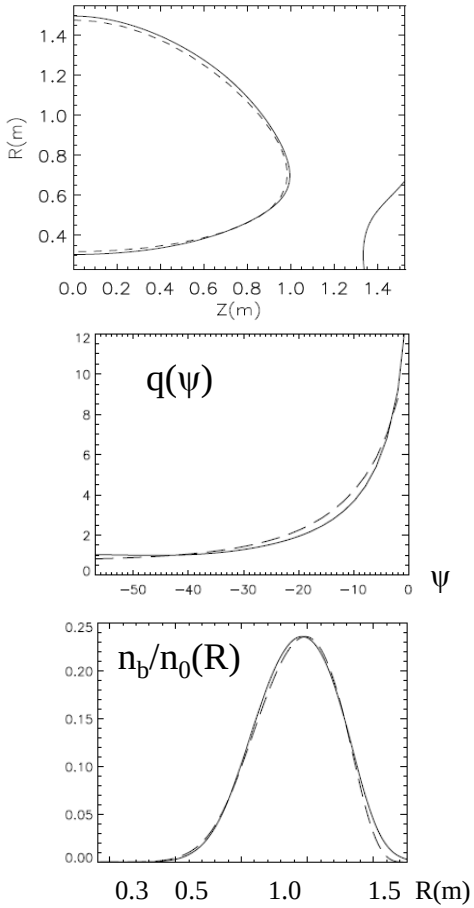

Plasma shape, q- and n_b profiles for NSTX-U shot 204707 t=0.44 from TRANSP and HYM GS solver + FREE_FIX.

$$F_{beam} \sim \exp(-(\lambda - \lambda_0(v))^2 / \Delta\lambda(v)^2)$$

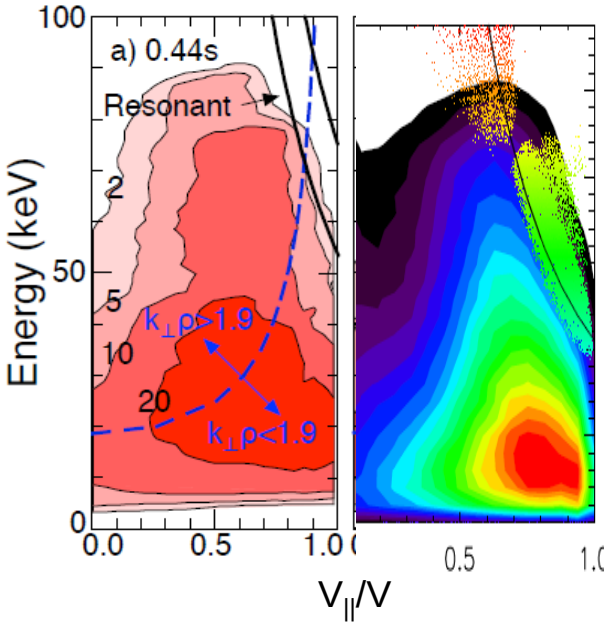

(a) TRANSP fast-ion distribution for t=0.44, resonant line for n=-11 GAE, estimated γ_{dr}~0.5%ω_{ci};
(b) HYM fast-ion distribution from n=-10 GAE simulations, γ_{dr}~2.5%ω_{ci}. Dots show resonant particles.

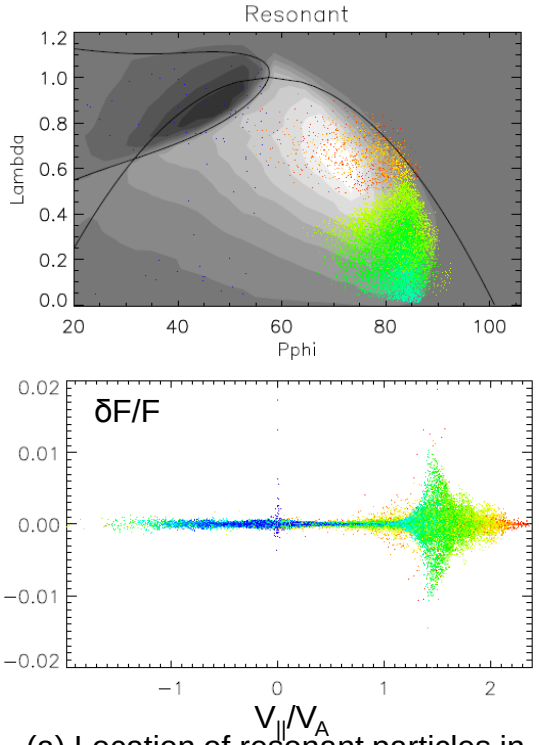

(a) Location of resonant particles in phase space: $\lambda=\mu B_0/\varepsilon$ vs p_φ.
(b) Particle weight w ~ δF/F vs orbit-averaged parallel velocity. Particle color corresponds to different energies: from E=0 (purple) to E=90keV (red).

PPPL PRINCETON PLASMA PHYSICS LABORATORY

High-frequency CAE/GAE studies: remaining issues/plans

- Improvement of the fast ion distribution function model (GAE/CAE).
- Understanding conditions for preferential excitation of GAEs and CAEs.
- Thermal ions kinetic effects (Hall, FLR) are important for CAE/KAW modeling.
- Bulk plasma rotation can have effect on GAE stability and mode structure.
- Finite $\delta E_{||}$ (generalized Ohm's law) is needed for accurate description of electron transport.
- Comparison of the relative importance of the energy channeling vs anomalous electron transport mechanisms.
- Comparison with experimental results including mode structure, saturation amplitudes and etc for several shots.

2D and 3D hybrid simulations of spheromak merging

PPPL
PRINCETON
PLASMA PHYSICS
LABORATORY

HYM model equations

Hybrid: Fluid electrons/Kinetic ions

$$\frac{\partial \mathbf{B}}{\partial t} = -c\nabla \times \mathbf{E},$$

$$\mathbf{E} = -\mathbf{v}_e \times \mathbf{B}/c - \nabla p_e/en_e + \eta \mathbf{J},$$

$$\mathbf{J} = c/4\pi \nabla \times \mathbf{B},$$

$$\mathbf{v}_e = -(\mathbf{J} - \mathbf{J}_i)/en_e,$$

$$\frac{\partial p_e}{\partial t} + \gamma p_e(\nabla \cdot \mathbf{v}_e) + \mathbf{v}_e \cdot \nabla p_e = \eta(\gamma - 1)J^2,$$

Ion trajectories calculated via Lorenz force

$$\frac{d\mathbf{x}}{dt} = \mathbf{v},$$

$$\frac{d\mathbf{v}}{dt} = \frac{q_i}{m_i}\left(\mathbf{E} - \eta\mathbf{J} + \mathbf{v} \times \mathbf{B}/c\right).$$

One fluid MHD

$$\frac{\partial \rho}{\partial t} + \nabla \cdot (\rho \mathbf{v}) = 0,$$

$$\frac{\partial \rho \mathbf{v}}{\partial t} = -\nabla \cdot (\rho \mathbf{v}\mathbf{v}) - \nabla p + \mathbf{J} \times \mathbf{B}/c + \mu \Delta \mathbf{v},$$

$$\partial p^{1/\gamma}/\partial t + \nabla \cdot (\mathbf{v} p^{1/\gamma}) = \frac{(\gamma - 1)}{\gamma} p^{1/\gamma - 1}\left[\eta J^2 + \mu(\nabla \times \mathbf{v})^2 + \mu(\nabla \cdot \mathbf{v})^2\right],$$

$$\partial \mathbf{A}/\partial t = -c\mathbf{E},$$

$$\mathbf{E} = -\mathbf{v} \times \mathbf{B}/c + \eta \mathbf{J}.$$

$$\mathbf{J} = c/(4\pi)\nabla \times \mathbf{B}$$

Hybrid simulations of counter-helicity spheromak merging

- Initial configuration, ie two spheromaks, was generated by solving Grad-Shafranov equation in half-region and reflecting solution anti-symmetrically relative to the midplane.

- Initial ion temperature was assumed to be small and uniform, and thermal ion Larmor radius was relatively small with ρ_i/R_c~0.014, where R_c is the flux conserver radius (MHD-like regime).

- Simulation particles were loaded with Maxwellian distribution and density consistent with the initial density profile.

- Option to include reconnection control coil at the midplane (RCC).

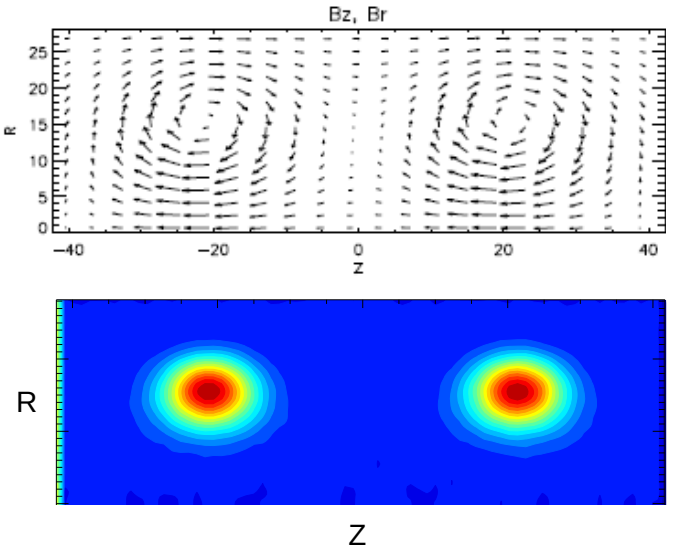

(a) Vector plot of initial poloidal magnetic field; (b) contour plots of ion density at t=0. Initial conditions for hybrid simulations of counter-helicity spheromak merging.

2D MHD vs Hybrid simulations with RCC

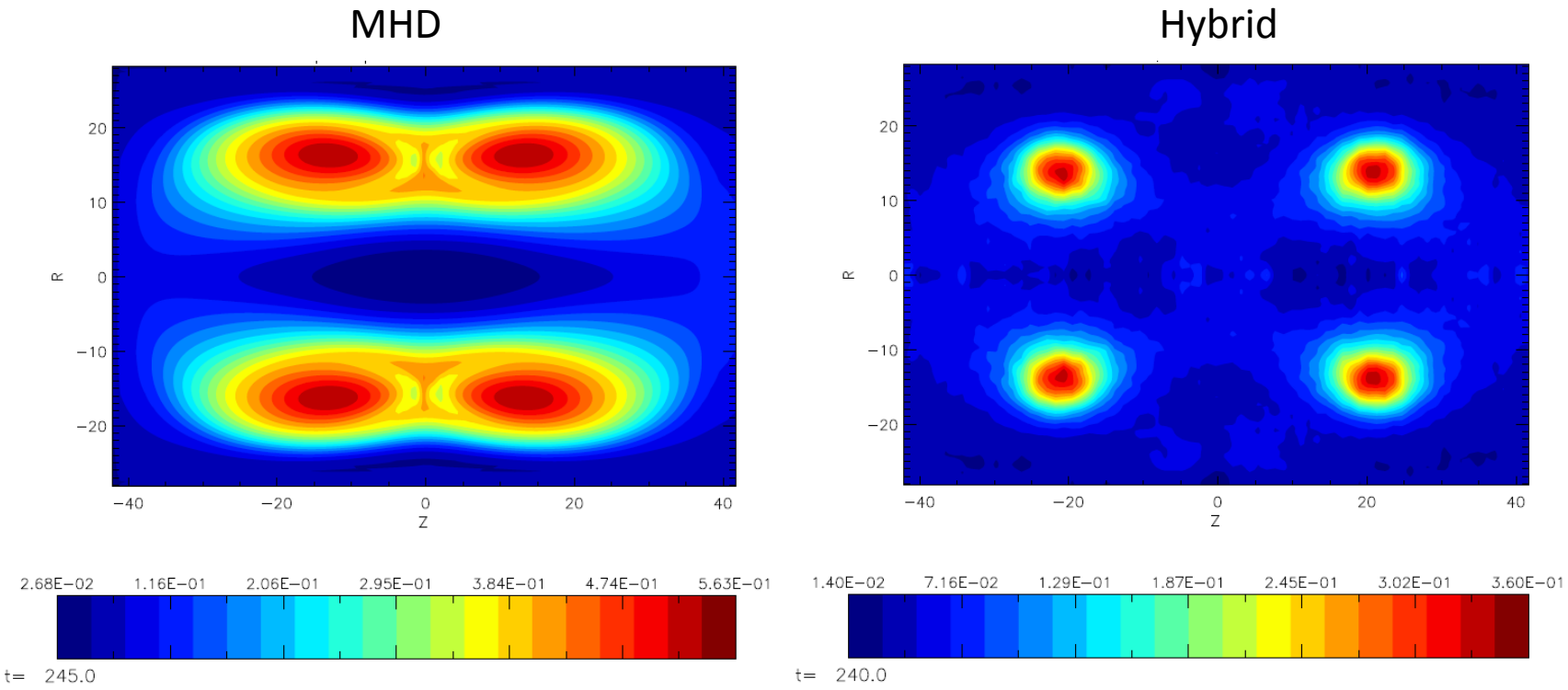

Contour plots of (a) plasma pressure from MHD simulations, and (b) ion pressure from 2D hybrid simulations of counter-helicity spheromak merging at $t=8.5t_A$.

Hybrid simulations with RCC

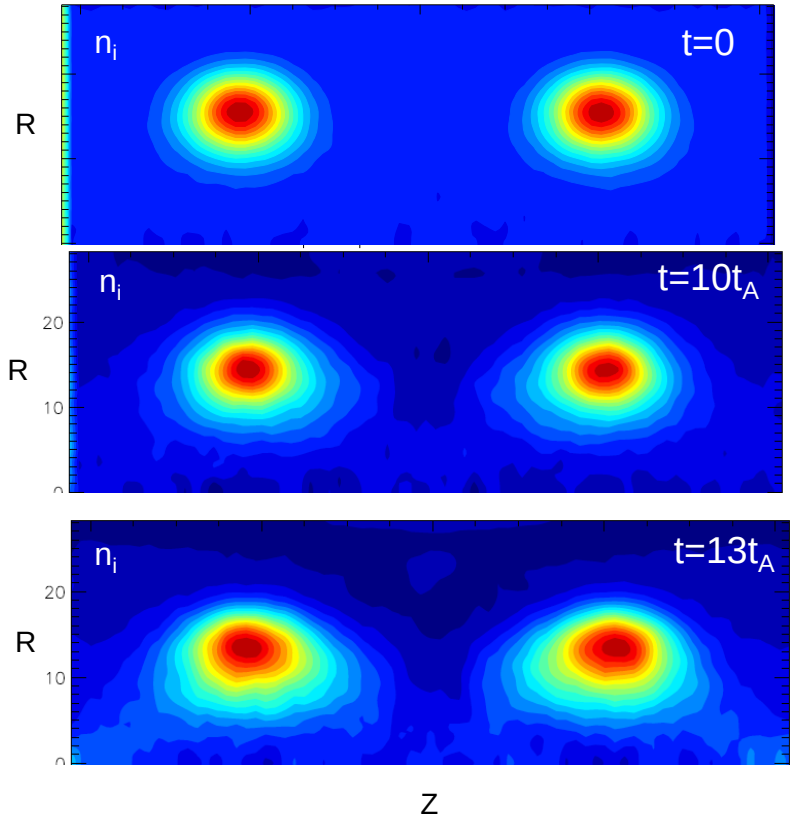

Contour plots of ion density from 2D hybrid simulations of counter-helicity spheromak merging.

In simulations with RCC (large resistivity, Lundquist number S~500), there were significant differences between hybrid and MHD simulations:

- in the MHD runs, spheromaks move towards the midplane, and merge completely in about $10t_A$,
- in hybrid simulations with the same plasma parameters, the spheromaks moved towards midplane initially, but then bounced back, and there were no complete reconnection.
- Unlike hybrid simulations, Hall-MHD simulations show global dynamics similar to that of MHD.

Hybrid simulations with no RCC

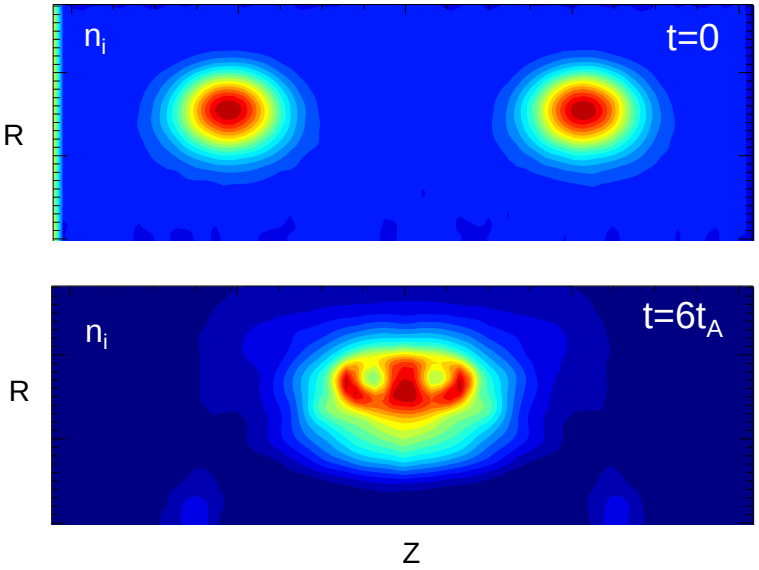

Contour plots of ion density at t=0 and $t=5.7t_A$. From 2D hybrid simulations of counter-helicity spheromak merging with S=1500.

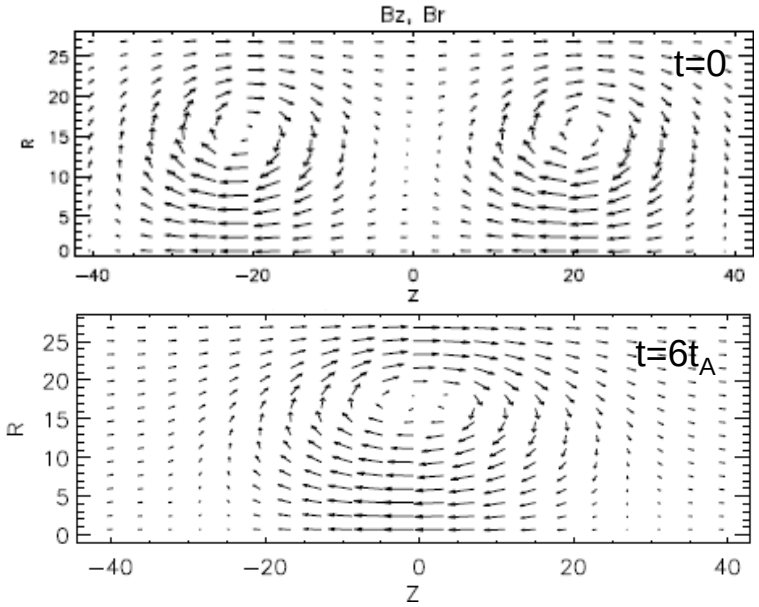

Vector plots of poloidal magnetic field at t=0 and $t=5.7t_A$.

Global dynamics in hybrid simulation was generally similar to the MHD simulations, and spheromaks were completely merged forming an FRC by $t\sim 6t_A$.

Comparison with MHD simulations

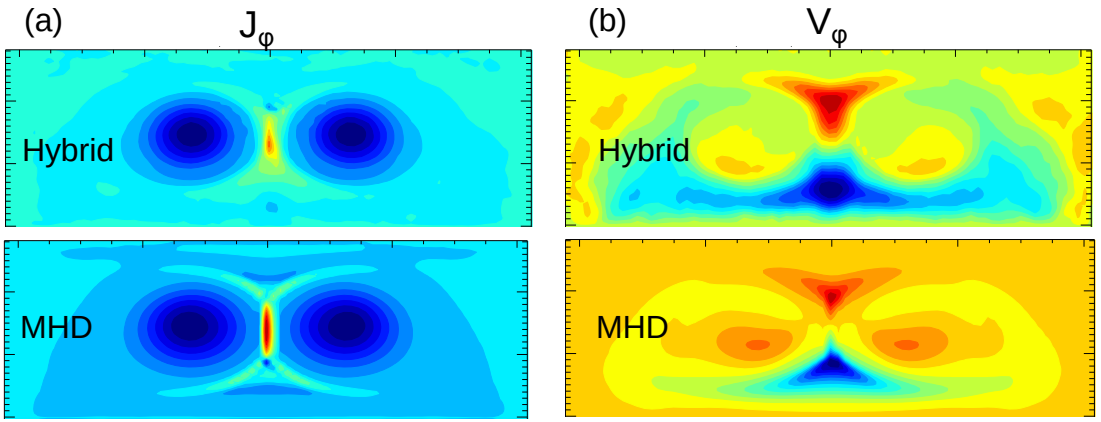

Contour plots of (a) toroidal current and (b) toroidal ion velocity from 2D hybrid simulations and 2D MHD simulations of counter-helicity spheromak merging.

- Hybrid simulations show shorter current layer.
- Significantly wider ion velocity profiles, probably due to large ion orbits near X-point.
- Hybrid simulations show outward radial shift of the reconnection X-point, which is related to generation of a quadrupole field, and has also been observed in 2D Hall-MHD simulations.

3D MHD simulations of counter-helicity spheromak merging

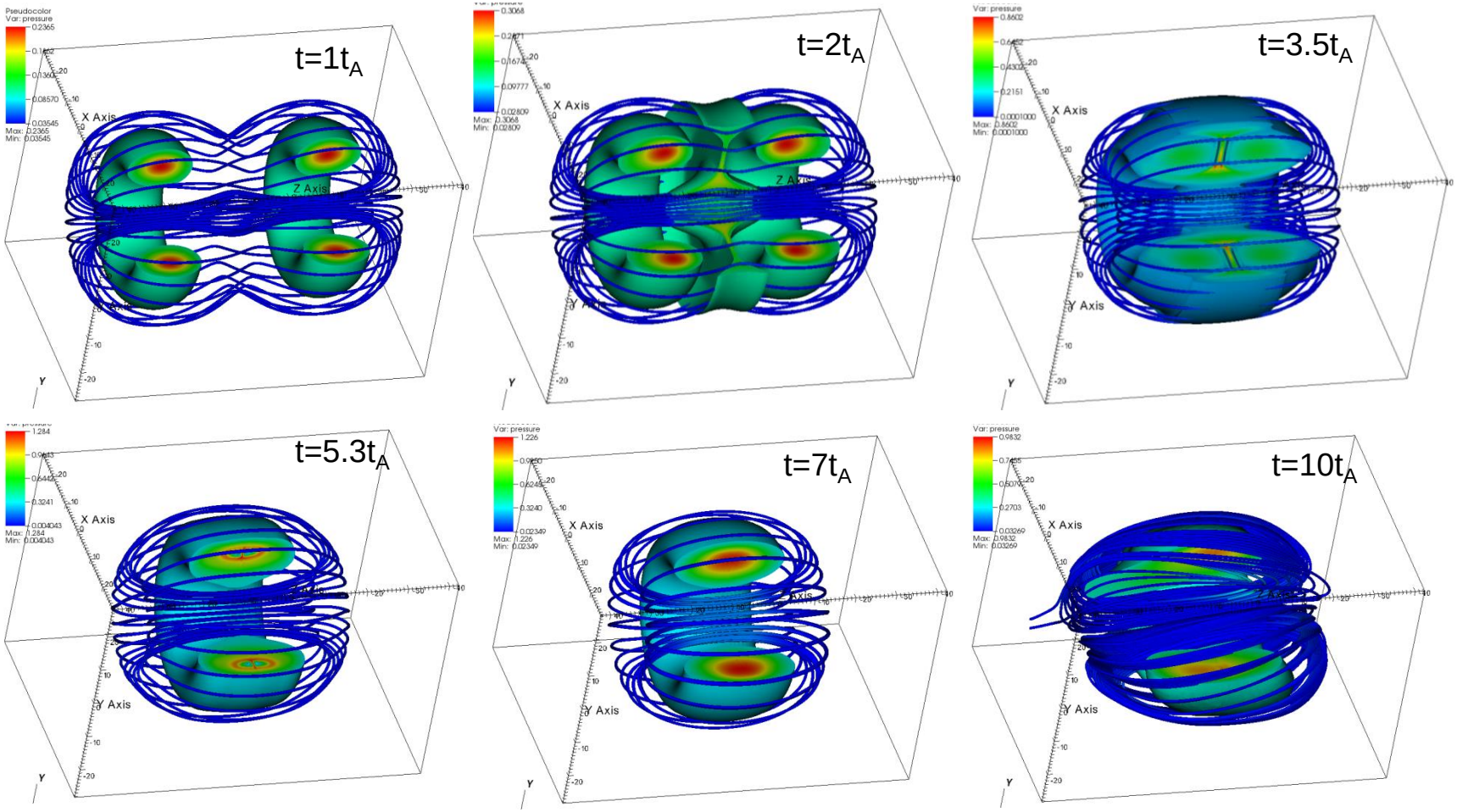

Magnetic field lines and contour plots of plasma pressure. Random initial perturbation at $0.01V_A$.

3D Hybrid simulations of counter-helicity spheromak merging

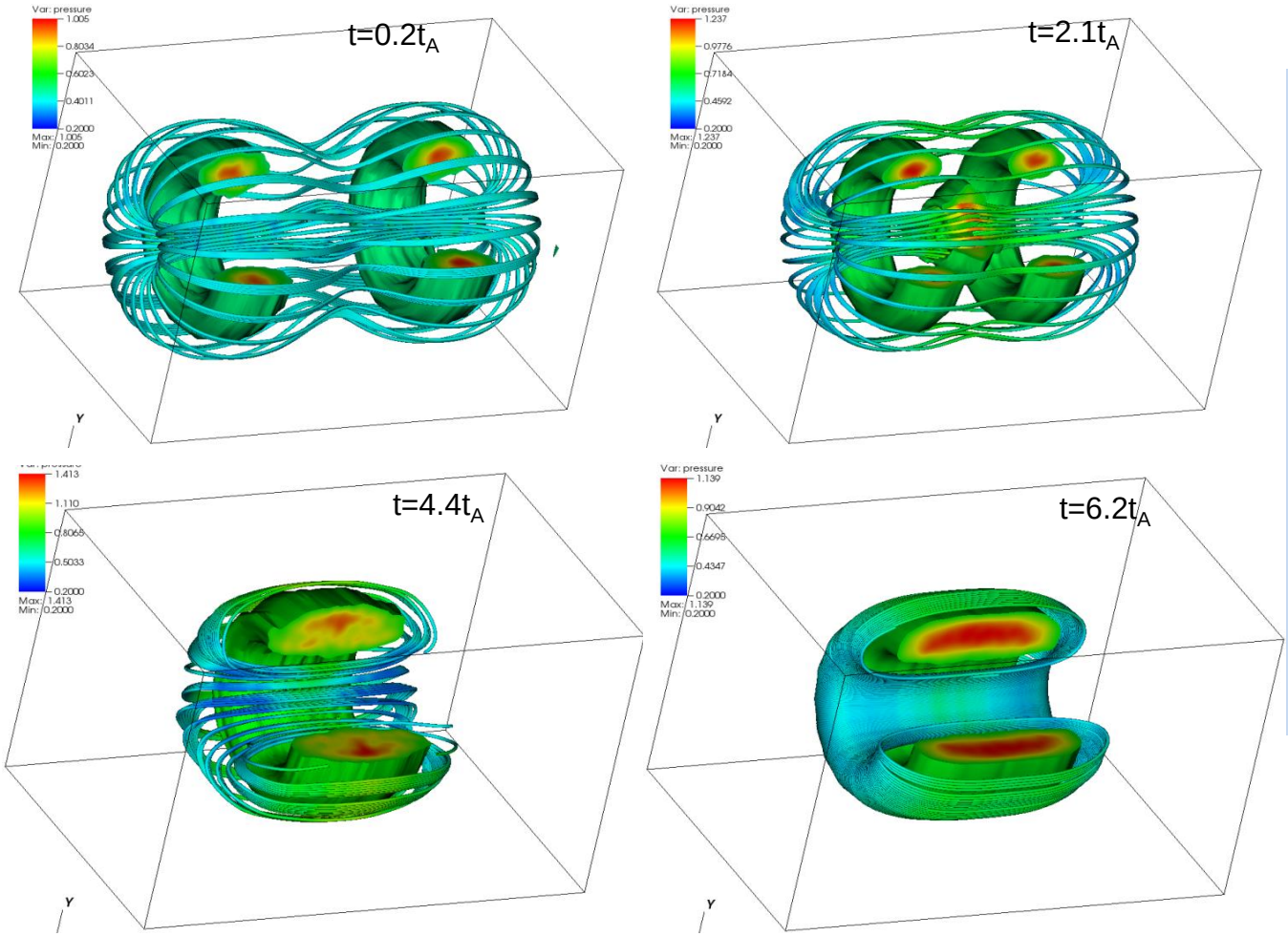

Magnetic field lines and contour plots of ion pressure. FRC forms with larger elongation and flatter pressure profile compared to MHD.

Small FLR, MHD-like regime.

- Without RCC (faster reconnection) 3D hybrid simulation are similar to MHD in terms of global dynamics.

- Differences between hybrid and MHD (Hall-MHD) simulations with RCC: in hybrid simulations there was no complete reconnection.

3D simulations: kinetic energy evolution - MHD vs hybrid

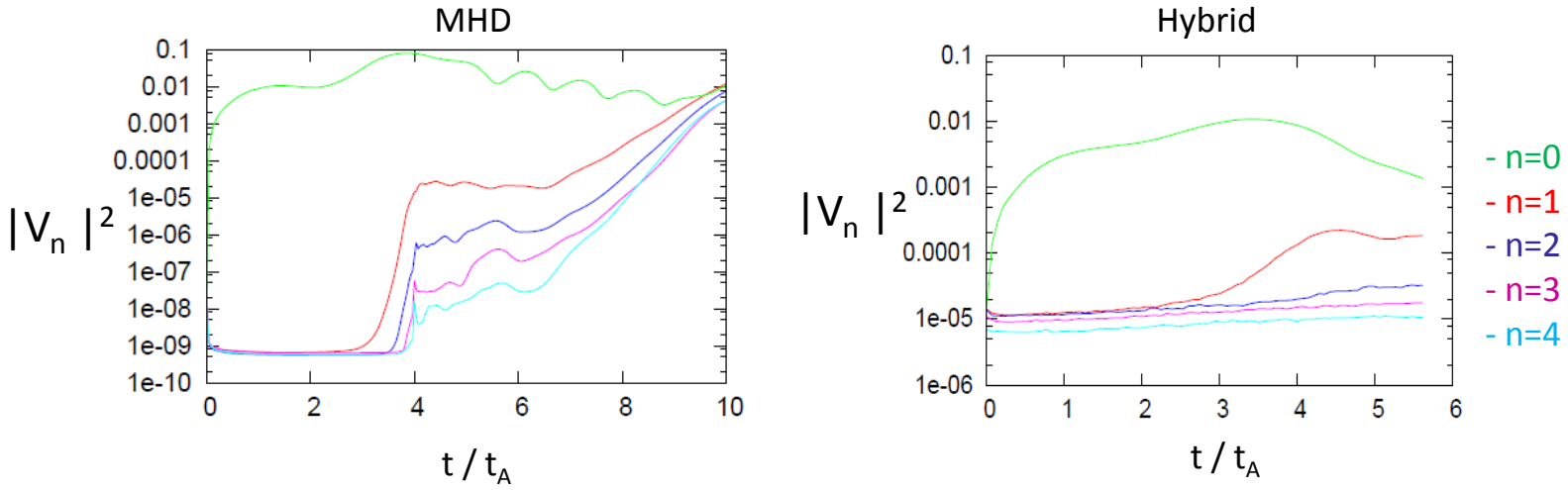

Time evolution of kinetic energy for different Fourier harmonics from 3D MHD and hybrid full-f simulations. Reconnection occurs at t~4-6t_A , and it is not axisymmetric – finite n=1 component.

- n=0 shows radial oscillations of FRC after formation (MHD).
- n=0 amplitude in hybrid run is smaller than in MHD.
- n=1 tilt mode (and higher n) grows after FRC formation (t>6t_A).

Summary

- There were significant differences between hybrid and MHD (Hall-MHD) simulations with RCC: in the MHD runs, spheromaks merged completely in about $10t_A$, whereas in hybrid simulations there was no complete reconnection.

- In cases without the RCC (faster reconnection) hybrid simulation results were similar to the MHD simulations in terms of global dynamics, and spheromaks were completely merged forming an FRC by $t\sim 6t_A$. 3D evolution is similar to MHD.

- Results are consistent with 2D full PIC and hybrid simulations of island coalescence, where it was found that fluid description including the Hall term does not describe reconnection in large systems correctly [1,2], unlike in the local current-sheet studies. It was shown that merging becomes increasingly ineffective for larger islands due to large gradients of the ion pressure tensor, broader ion diffusion region, and reduced outflow velocities [2].

[1] H. Karimabadi, et al., PRL**107**, 025002 (2011); A. Stanier et al., PRL.**115**, 175004 (2015).
[2] J. Ng, et al., Phys. Plasmas **22**, 112104 (2015).